

UAV-based thermal imaging in the assessment of water status of soybean plants

Luís Guilherme Teixeira Crusiol, Marcos Rafael Nanni, Renato Herrig Furlanetto, Rubson Natal Ribeiro Sibaldelli, Everson Cezar, Liliane Marcia Mertz-Henning, Alexandre Lima Nepomuceno, Norman Neumaier & José Renato Bouças Farias

To cite this article: Luís Guilherme Teixeira Crusiol, Marcos Rafael Nanni, Renato Herrig Furlanetto, Rubson Natal Ribeiro Sibaldelli, Everson Cezar, Liliane Marcia Mertz-Henning, Alexandre Lima Nepomuceno, Norman Neumaier & José Renato Bouças Farias (2020) UAV-based thermal imaging in the assessment of water status of soybean plants, International Journal of Remote Sensing, 41:9, 3243-3265, DOI: [10.1080/01431161.2019.1673914](https://doi.org/10.1080/01431161.2019.1673914)

To link to this article: <https://doi.org/10.1080/01431161.2019.1673914>



Published online: 08 Oct 2019.



Submit your article to this journal [↗](#)



Article views: 208



View related articles [↗](#)



View Crossmark data [↗](#)



UAV-based thermal imaging in the assessment of water status of soybean plants

Luís Guilherme Teixeira Crusiol ^a, Marcos Rafael Nanni ^a, Renato Herrig Furlanetto^a, Rubson Natal Ribeiro Sibalidelli^b, Everson Cezar^a, Liliane Marcia Mertz-Henning^c, Alexandre Lima Nepomuceno^c, Norman Neumaier^c and José Renato Bouças Farias^c

^aDepartment of Agronomy, State University of Maringá, Maringá, Brazil; ^bMathematician, Statistical Specialist, Londrina, Brazil; ^cEmbrapa Soja, National Soybean Research Centre – Brazilian Agricultural Research Corporation, Londrina, Brazil

ABSTRACT

Soybean production both in Brazil and globally has regularly been threatened by drought periods. The use of infrared thermography to evaluate the canopy's temperature and its relationship with plant water status constitutes an important tool for agricultural monitoring. However, studies regarding the water status of soybean plants through unmanned aerial vehicle (UAV)-based thermal imaging are yet to be reported. Thus, the present study aimed to evaluate the water status of soybean plants submitted to different water conditions via thermal images obtained through an UAV thermal infrared camera. The field experiment was undertaken at the National Soybean Research Centre (Embrapa Soja, a branch of the Brazilian Agricultural Research Corporation) in a randomized complete block design, with four replicates. The following water conditions were evaluated: irrigated (IRR, receiving rainfall and irrigation when necessary, and with a soil water matric potential between -0.03 MPa and -0.05 MPa), non-irrigated (NIRR, receiving only rainfall), and water deficit (or drought stress) induced at the vegetative (DSV) and reproductive (DSR) stages. Water deficit was induced using rainout shelters. Soil moisture and weather data were monitored daily. Thermal images were obtained on twelve dates, half in 2016–2017 and half during the 2017–2018 crop seasons, through a thermal infrared camera (DIY-Thermocam) sensitive to temperatures ranging from -40°C to 200°C , with 0.5°C accuracy and 14-bit radiometric resolution. Images in RAW format (160 pixels \times 120 pixels) were obtained at 125 m above ground level. They were then processed and calibrated by acquiring a correction factor resulting from the effect of atmospheric attenuation. The canopy temperature was evaluated in relation to that of air temperature and through the Normalized Relative Canopy Temperature (NRCT). Atmospheric attenuation was positively correlated to flight altitude, so that image correction eliminated such an effect. The thermal behaviour of soybean plants was directly correlated to soil water availability and atmospheric vapour pressure deficit, with differences ranging from 0.2°C to 7.2°C . Plants grown at lower soil moisture conditions had higher temperatures, which were

ARTICLE HISTORY

Received 20 February 2019
Accepted 20 June 2019

observed under DSV and DSR conditions. However, plants submitted to DSV and then rehydrated under normal field conditions demonstrated lower temperatures than those presented by plants under IRR or NIRR. Water deficit was more damaging to yields when induced at the reproductive stage. We emphasize the potential use of UAV thermal infrared cameras for monitoring the water status of soybean plants, and for collecting non-destructive information in support of better crop management decisions and new studies.

1. Introduction

Brazil is one of the world's largest soybean producers. In the 2017–2018 crop season, Brazilian soybean production was estimated at 115 million tons, representing over one third of the total global estimate of 335 million tons (CONAB (National Company of Food Supply) 2018; United States Department of Agriculture (USDA) 2018). However, soybean production in Brazil (and elsewhere) has regularly been threatened by the occurrence of unfavourable weather events, especially drought periods. Sentelhas et al. (2015) reported that water deficit has impaired around 30% Brazilian soybean production and caused financial losses of over US\$79 billion in 38 years (Ferreira 2016).

The use of infrared thermography to evaluate canopy temperature and its close relationship with plant water status has been reported for several decades (Gates 1964; Idso et al. 1981; Jackson et al. 1981; Mengistu et al. 1987). This relationship owes to stomatal closure under drought conditions, leading to lower transpiration rates and subsequently lower heat dissipation, resulting in canopy temperatures that are higher than those of air and plants under conditions of good water availability (Idso et al. 1981; Jackson, Kustas, and Choudhury 1988; Stolf-Moreira et al. 2011; Carvalho et al. 2015).

An increasing use of thermal infrared cameras can be observed today, especially attached to unmanned aerial vehicles (UAVs). These thermal cameras possess the advantage of rapid and non-destructive data collection, with the acquisition of reliable values. Furthermore, they provide the geographical location of the imaged phenomena, which represents a new acquisition platform of thermal data, attained in the past through handheld infrared thermometers, by which relatively few plants could be sampled, precluding the spatialization of results.

In this sense, studies correlating inflight- and UAV-obtained aerial thermal images to the water status of different crops are rather distinctive, and have been based in sites such as vineyards (Baluja et al. 2012; Zarco-Tejada et al. 2013; Bellvert et al. 2014, 2015), olive orchards (Sepulcre-Cantó et al. 2006; Berni et al. 2009a), fruit trees (Berni et al. 2009b; Zarco-Tejada, González-Dugo, and Berni 2012; Gonzalez-Dugo et al. 2013), corn (Berni et al. 2009b), and cotton fields (Sullivan et al. 2007).

Several authors have discussed the relationship between canopy temperature and water status in the soybean crop (Rao 1985; Mengistu et al. 1987; Carvalho et al. 2015; Crusiol et al. 2017). However, studies regarding the water status of soybean plants through UAV-based aerial thermal imaging are yet to be reported.

Thus, the present study aimed to evaluate the water status of soybean plants submitted to different water conditions by thermal images obtained through an UAV thermal infrared camera, which represents an issue that has yet to be addressed by any scientific journal.

2. Material and methods

2.1. Experimental site

The experiment (Figure 1) was conducted at the experimental farm of the National Soybean Research Centre (Embrapa Soja), a branch of the Brazilian Agricultural Research Corporation located in Londrina Municipality, Paraná State, Southern Brazil ($23^{\circ} 11' 37''$ S, $51^{\circ} 11' 03''$ W, 630 m above sea level). The study area has a Cfa climate according to the Köppen climate classification, i.e., subtropical climate, with a mean temperature in the hottest month higher than 22°C , and rainfall concentrated in the summer months, which corresponds to the period of soybean production, albeit with no defined dry season (Wrege et al. 2011; Alvares et al. 2013). Although dry season is not observed in the entire soybean crop season, large yield losses are often provoked by periods of water deficit (Sentelhas et al. 2015).

Experimental practices followed soybean production technologies (Embrapa Soja 2013). The experimental layout comprised a randomized complete block design, with four replicates. The following water conditions were evaluated: irrigated (IRR, receiving rainfall and irrigation when necessary, with a soil water matric potential between -0.03 MPa and -0.05 MPa), non-irrigated (NIRR, receiving only rainfall), and water deficit induced at the vegetative (DSV) and reproductive (DSR) stages.

DSV and DSR plots were established under rainout shelters programmed to cover plants (at the vegetative or reproductive stage) when rainfalls above 0.1 mm were recorded by the

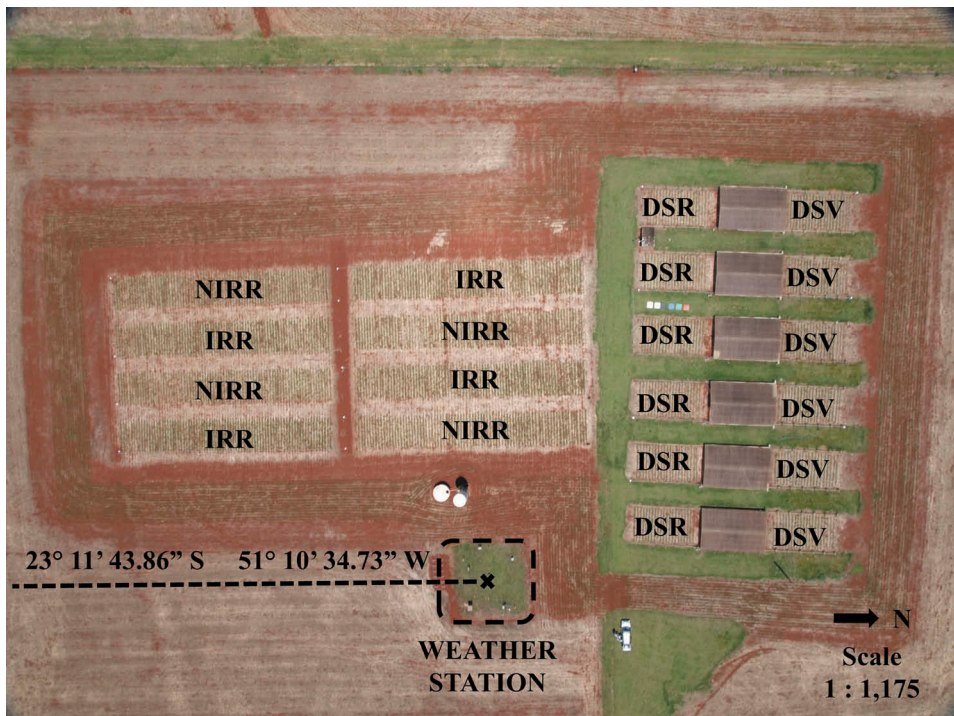


Figure 1. Experimental area showing the weather station and plots of the treatments: irrigated (IRR), non-irrigated (NIRR) and water deficit induced at vegetative (DSV) and reproductive (DSR) stages. Colour (RGB) image obtained 28 days after sowing through an UAV visible digital camera.

weather station located within the experimental area, thus simulating water deficit. Such plots had concrete barriers (90 cm depth) to prevent the lateral movement of water in the soil from outside to inside. Shelters automatically uncovered plants once rainfalls had ceased.

During the 2016–2017 crop season, sowing was performed on 19 October 2016, and the DSV treatment was induced from 25 November 2016 to the beginning of the flowering period (12 December 2016). From this date to the harvesting period, the DSR treatment was induced in previously rain-watered plots. In turn, the DSV plots began to be rain-watered, as shown in Figure 2(a).

Soil moisture (0 cm – 20 cm and 20 cm – 40 cm depths) was monitored daily on IRR plots by tensiometers, and in all other plots by gravimetric analysis on 24 November 2016, 16 December 2016, 9 January 2017, and 8 February 2017.

During the 2017–2018 crop season, sowing was performed on 18 October 2017, and the DSV treatment was induced from 20 November 2017 to the beginning of the flowering period (19 December 2017). From this date to the harvesting period, the DSR treatment was induced in previously rain-watered plots. In turn, the DSV plots began to be rain-watered, as shown in Figure 2(b).

Soil moisture (0 cm – 20 cm and 20 cm – 40 cm depths) was monitored daily on IRR plots by tensiometers, and in all other plots by gravimetric analysis on 4 December 2017, 14 December 2017, 22 January 2018, 1 February 2018, and 7 February 2018.

Weather data – comprising air temperature, relative air humidity and rainfall – were monitored by the weather station located within the experimental area, according to

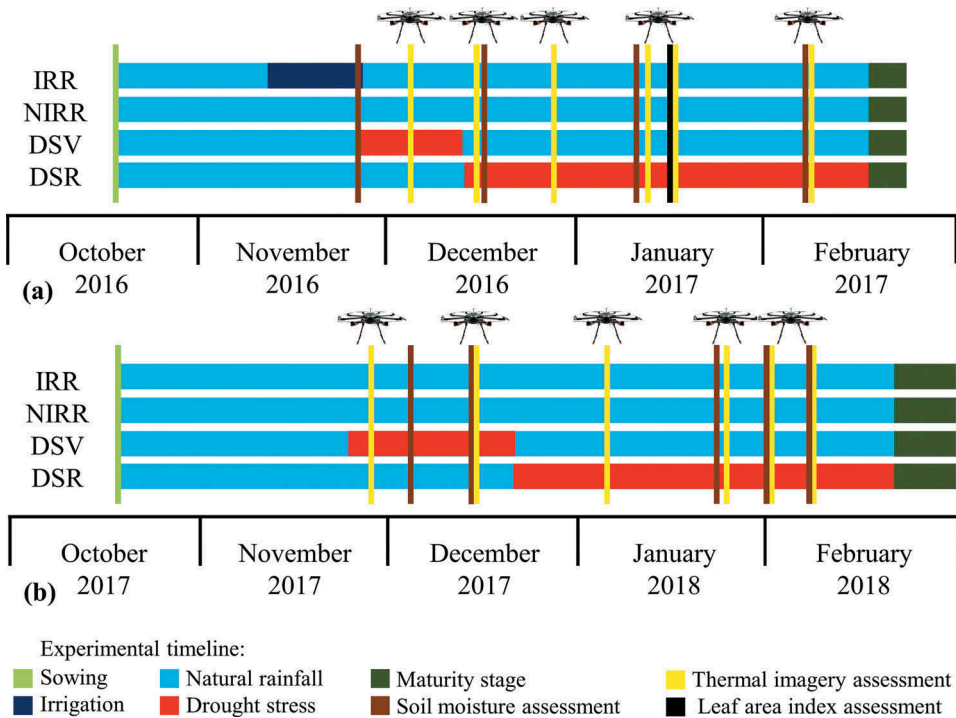


Figure 2. Experimental timeline, with evaluation dates on 2016–2017 (a) and 2017–2018 (b) crop seasons. Londrina-PR.

Sibaldelli and Farias (2017, 2018), and the climatic water balance was calculated (Thornthwaite and Mather 1955). Vapour pressure deficit (VPD) was obtained according to Equation (1):

$$VPD = \frac{(100 - RH)}{(100 \times e_s)}, \quad (1)$$

in which RH = relative air humidity and e_s = saturated vapour pressure (kPa), calculated through the Tetens equation (Tetens 1930).

The growth stages of the soybean plants were weekly monitored from emergence to maturation according to Fehr and Caviness (1977).

Leaf area index (LAI) was measured on 16 January 2017 as the ratio between the total one-sided area of leaf tissue per unit ground surface area, as per Equation (2) (Watson 1947):

$$LAI = \frac{T}{G}, \quad (2)$$

in which LAI is the leaf area index, T the total one-sided area of leaf tissue (m^2) and G the ground area occupied by a plant (m^2).

Grain yield was calculated and corrected for 13% grain moisture, as per Equation (3):

$$GY = \frac{(100 - H)}{(100 - D)} \times W \times \frac{10,000}{A}, \quad (3)$$

in which GY is the grain yield ($Kg\ ha^{-1}$), H the harvested grain moisture (%), D the desired grain moisture (%), W the harvested grain weight (Kg) and A the harvested plot area (m^2). Harvest grain moisture was measured using the G810 grain moisture metre (Gehaka Inc.).

2.2. Thermal image acquisition and processing

Thermal images were acquired on twelve dates during both the 2016–2017 and 2017–2018 crop seasons, always around midday and under sunny-sky conditions. In the 2016–2017 crop season, thermal image acquisition was undertaken in 2016 on 2, 15 and 27 December and in 2017 on 11 and 16 January and 8 February. In the 2017–2018 crop season, thermal images were acquired in 2017 on 29 November and 14 December, and 2018 on 4 and 25 January and 1 and 7 February. Images were captured through an UAV thermal infrared camera DIY-Thermocam (Ritter 2017), as displayed in Figure 3.

The camera operates at 7.5–14 μm spectral range and is sensitive to temperatures ranging from $-40^\circ C$ to $200^\circ C$, with $0.5^\circ C$ accuracy and 14-bit radiometric resolution (16,384 digital numbers). Images in 'RAW' format (160 pixels \times 120 pixels) were obtained at 125 m above ground level (AGL), with spatial resolution of 0.80 m. The spatial resolution deeply depends on flying height, and for thermal sensors it is, in general, lower than red-green-blue (RGB) sensors (Maes, Huete, and Steppe 2017). Faye et al. (2016) have discussed that thermal sensors with spatial resolution lower than 1 m are suitable for vegetation studies and reported the contribution of the background emissivity on the vegetation temperature and the importance of selecting pure pixels of the canopy.

Prior to image acquisition, the sensor was properly preheated in order to eliminate undesirable variations soon after being activated.

One thermal image containing all plots of the experimental area was selected from each evaluation date to minimize error sources, including changes in surface temperature



Figure 3. Unmanned aerial vehicle (UAV) equipped with a set of cameras (thermal, visible and near-infrared) flying over experimental plots.

and weather conditions, as frequently observed in evaluations using a mosaic of aerial images (Maes, Huete, and Steppe 2017).

Following acquisition, the images were processed using the software ThermoVision_Joe-C, version 1.3.0.2 (Ritter 2017). Images in ‘RAW’ format were converted into thermal images. Furthermore, the temperature values of each image were corrected. Subsequently, the temperature values were extracted from pure pixels referring to the canopies of experimental plots. For that propose an RGB image was combine to the thermal one, which guarantee the identification of vegetation pure pixels.

Canopy temperature (T_c) was evaluated in relation to air temperature (T_a) (Sepulcre-Cantó et al. 2006; Zarco-Tejada, González-Dugo, and Berni 2012; Carvalho et al. 2015; Crusiol et al. 2017) and through the Normalized Relative Canopy Temperature – NRCT (Elsayed, Rischbeck, and Schmidhalter 2015) according to Idso et al. (1981). NRCT was calculated according to the Equation (4):

$$\text{NRCT} = \frac{T_c - T_{\text{wet}}}{T_{\text{dry}} - T_{\text{wet}}}, \quad (4)$$

in which T_c represents canopy temperature, T_{wet} represents the lowest temperature among all treatments, assuming that these plants were under maximal transpiration conditions, and T_{dry} represents the highest temperature among all treatments, assuming that these plants were under minimal transpiration conditions. NRCT ranges from 0 to 1, hence drought stress is more severe at values closer to 1.

The NRCT is similar to the Canopy Water Stress Index – CWSI. For the calculation of the CWSI the values of T_{wet} and T_{dry} are obtained based on theoretical models, considering the relationship between canopy temperature for each crop and weather variables, especially VPD. Jackson et al. (1981), (1988) stated that other weather variables might influence CWSI, such as solar radiation and wind speed. Therefore, by assuming that T_{wet} represents the

lowest canopy temperature and T_{dry} the highest within the field trial for the calculation of the NRCT, real and reliable values regarding the highest and lowest effective transpiration capacity of plants under weather conditions during the evaluation period are ensured, because all plants exist under the same conditions of air temperature, relative air humidity, solar radiation, wind speed and direction, soil class, and planting system. Only water availability was effectively modified, resulting in different soil moisture values. This procedure has been applied either partially or totally in previous studies, and has produced valid results (Jones 1999; Jones et al. 2002; Elsayed et al. 2017; Elvanidi et al. 2017; Gonzalez-Dugo et al. 2013; Alchanatis et al. 2010).

2.2.1. Thermal correction

UAV thermal cameras are typically small in order to ensure they can be transported by air. Therefore, many thermal cameras, as the one used in this study, are often equipped with a microbolometer (uncooled thermal sensor), which results in frequent changes in their internal response (Gómez-Candón et al. 2016). Furthermore, thermal radiation attenuation by gases and atmospheric suspended particles can lead to a decline in values recorded by the sensor in relation to the real temperature of imaged targets (Lillesand, Kiefer, and Chipman 2004). For these reasons, the temperature of UAV-based thermal images must always be corrected.

An experiment was thus undertaken in order to set a procedure for the correction of UAV-based thermal images. Four plots (10 m × 10 m) of a homogenous planting surface (lawn) and six tarpaulins (5 m × 5 m) of different shades were used as correction patterns.

Thermal images were captured between 1 m and 400 m AGL at 25 m intervals. Simultaneously with aerial thermal imaging, the temperature was measured on each tarpaulin and lawn plot via an InfraPro® infrared thermometer (Oakton®).

As a result, the following items were calculated: the Pearson correlation coefficient between the infrared thermometer and the thermal camera at 100 m AGL; the Pearson correlation coefficient (r) between the flight altitude of UAV and the temperature recorded by the thermal camera; the mean lawn temperature recorded by the thermal camera at 1 and 100 m AGL; and the difference between the temperature measured at 1 m AGL (reference temperature) and at 100 m AGL, in the same reference targets, hence obtaining a correction factor resulting from the effect of thermal radiation attenuation by the atmosphere. The correction factor was applied to images obtained at each flight altitude (AGL) and the temperature values were extracted, again calculating the mean lawn temperature recorded by the thermal camera at each flight altitude (AGL) after correction, according to Equation (5):

$$T_{cor} = T_{flight} + (T_{ref} - T_{flight}) \quad (5)$$

in which T_{cor} = temperature of the thermal image after correction, T_{flight} = temperature of the thermal image at each flight altitude (AGL) and T_{ref} = temperature of the thermal image measured at 1 m AGL.

Subsequently, in each evaluation period (twelve in total) of soybean plants, an image was captured at 1 m AGL, enabling the correction factors to be acquired for their respective aerial images.

2.3. Unmanned aerial vehicle – UAV

A Tarot Iron Man 1000 octocopter was used (Figure 3), structurally composed of 3k carbon fibres, equipped with brushless T-Motors, model MN5212, 340 kv and 600 W power per axis, and holding 3k carbon fibre propellers measuring 43.18 cm × 13.97 cm. Its payload capacity was 4 kg and its flight autonomy measured approximately 20 minutes using a lithium-polymer battery (LiPo) of 16.000 mAh, 6 S, 22.8 V. It had a discharge rate of 10 C, enabling the UAV to transport several sensors at the same time. A camera stabilization system was developed in order to avoid vibrations during aerial imagery.

An autopilot system 3D Robotics model Pixhawk with two 32 bit processors Cortex M4 (128 MHz) and a stabilization system with gyroscope (ST Micro L3GD20H 16 bit), xyz-axis accelerometer (InvenSense MPU-6000) and barometer (MEAS MS5611) with 10 cm stabilization accuracy in z-axis were used to control the UAV. The absolute positioning of the UAV was guaranteed by an Ublox LEA-6H GPS with high precision.

Aerial imagery was planned by the Mission Planner software. At the ground station, a Futaba T14SG transmitter operating at 2.4 GHz frequency and a FASSTest protocol for data transmission to the UAV were used. Image capture, communication, position, altitude, and time-of-flight data were obtained by telemetry operating at 900 MHz frequency. A first-person view (FPV) transmission system of 5.8 GHz was used for the live monitoring of the flight and made corrections in the positioning of the UAV over the experiment as required.

2.4. Statistical analysis

Once the assumptions of the analysis of variance (ANOVA) had been met, the data were submitted to ANOVA and means compared by the Tukey test ($p \leq 0.05$) via the software Sisvar (Ferreira 2011).

3. Results and discussion

3.1. Temperature correction of thermal images

Figure 4(a) shows the Pearson correlation coefficient (r) between the infrared thermometer, operated at ground level ($T_{\text{infrared thermometer}}$), and the thermal camera ($T_{\text{thermal camera}}$), operated at 100 m AGL. A strong positive correlation was observed between the two sensors. The regression analysis with an intersection passing through the origin ($y = bx$) revealed an adjusted model ($y = 0.7276x$) with coefficients of determination (R^2) and correlation (r) equal to 0.9309 and 0.9786, respectively. Although the values measured by the two sensors presented a linear correlation close to the maximum (1), the temperatures obtained through the UAV thermal infrared camera were slightly lower than those measured by the infrared thermometer, based on the slope (0.7276), which indicates such a trend (Figure 4(a)).

In this sense, Figure 4(b) illustrates the Pearson correlation coefficient between temperatures and flight altitudes for thermal image acquisition. The coefficients of determination and correlation equal to 0.9324 and 0.9656, respectively, indicate that an increase in altitude leads to a decline in the temperature values recorded by the sensor. Thus, such values must be corrected in order to integrate thermal data from different targets, resulting in reliable values even when imaged at different altitudes and under different atmospheric conditions.

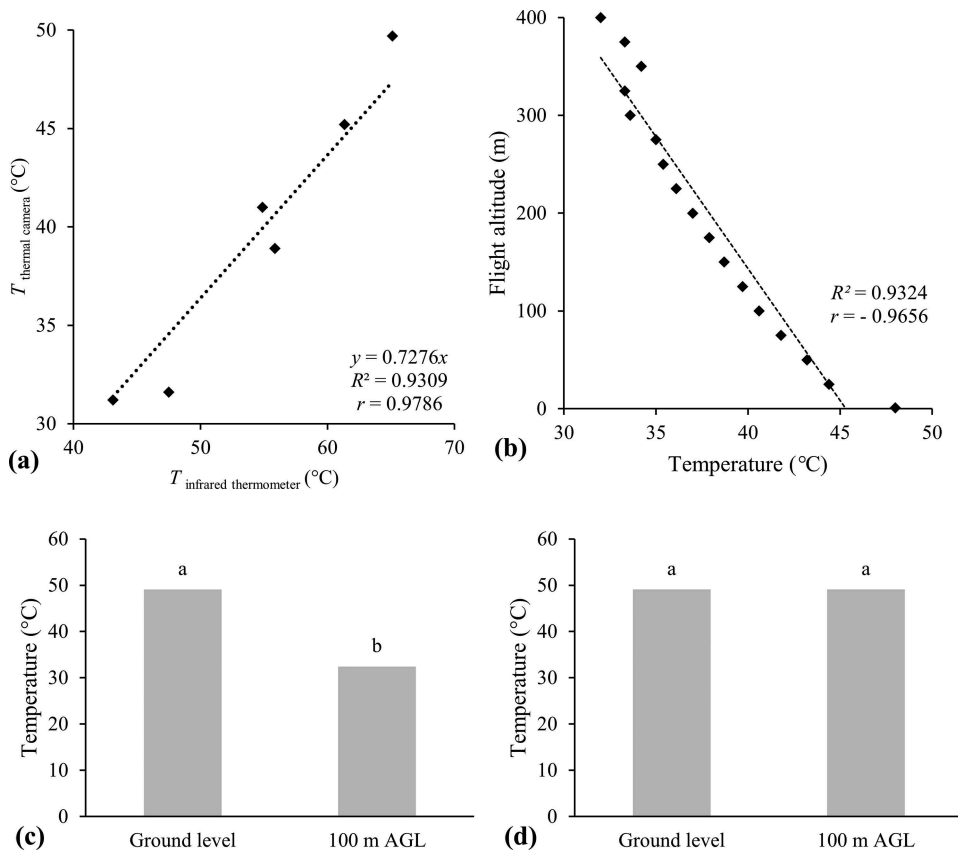


Figure 4. Pearson correlation coefficient between temperature measured by an infrared thermometer at ground level ($T_{\text{infrared thermometer}}$) and by an UAV thermal infrared camera ($T_{\text{thermal camera}}$) at 100 m AGL (a); Pearson correlation coefficient between flight altitude and temperature measured by an UAV thermal infrared camera (b); lawn temperature obtained through a thermal camera at ground level and at 100 m AGL, before (c) and following the application of a correction factor (d). Means followed by the same letter do not differ by Tukey test ($p \leq 0.05$).

Figure 4(c) shows that the canopy temperature obtained at 1 m AGL had values that were significantly higher than those obtained at 100 m AGL, with around 16°C mean difference. Following the application of a correction factor directly related to atmospheric attenuation (Equation (4), Figure 4(d)), differences between the readings performed at these altitudes were eliminated, thus preventing the misinterpretation of thermal data. In this way, on each date of imaging of soybean plants, an image was captured at 1 m AGL in addition to that obtained at 125 m AGL, enabling the correction factor to be calculated and Equation (4) to be applied, ensuring the data's reliability as a result.

3.2. Canopy temperature and NRCT

Figure 5 displays the canopy temperature and NRCT data obtained through an UAV thermal infrared camera during the 2016–2017 crop season. Regarding the treatments

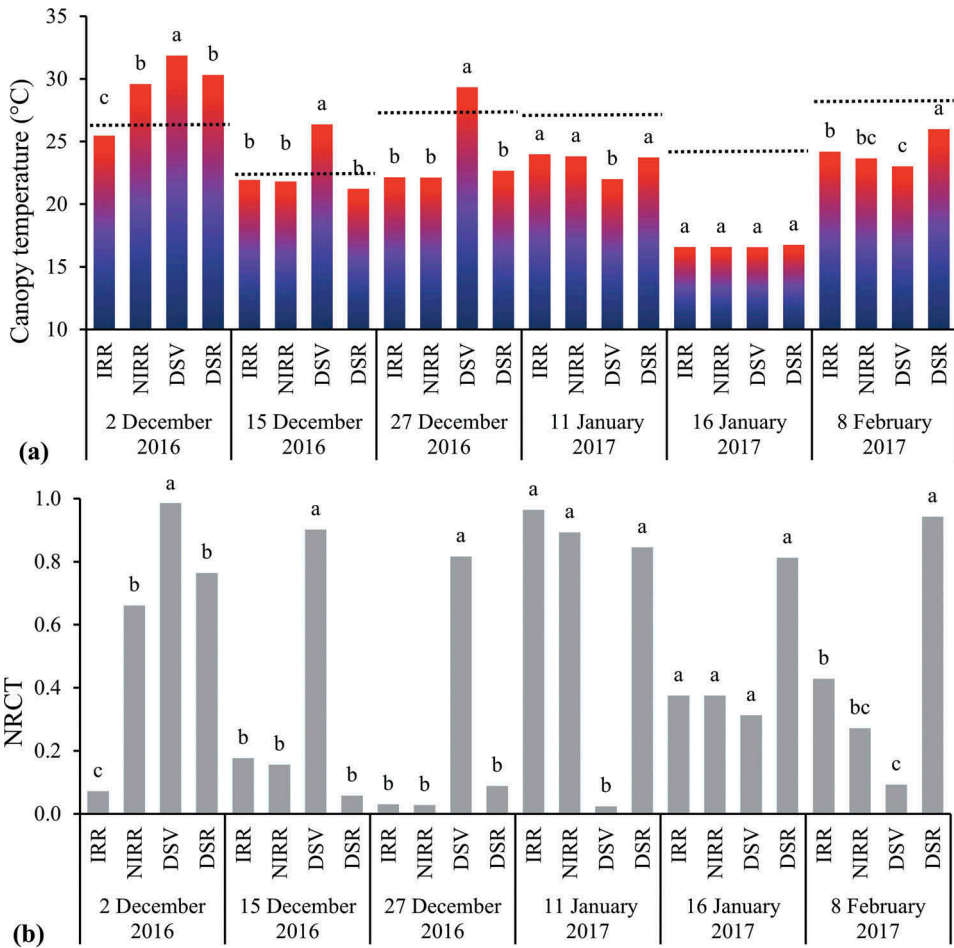


Figure 5. Canopy temperature (a) and NRCT (b) during the 2016–2017 crop season. Dashed lines represent air temperature (°C) on each date. Means followed by the same letter among treatments within each date do not differ by Tukey test ($p \leq 0.05$).

evaluated, the NRCT and canopy temperature revealed the same trend, which was to be expected given that the former is derived from the latter. However, by using different forms of temperature evaluation (canopy temperature and NRCT) and presenting the resulting data side-by-side, the data can be more clearly understood.

The evaluation of canopy temperature in relation to air temperature renders it possible to understand environmental conditions during image acquisition, as real differences between canopy (T_c) and air (T_a) temperatures and among the T_c of evaluated treatments can be highlighted. In turn, given that NRCT is a normalized index ranging from 0 to 1, it applies a contrast on the data evaluated, enabling small temperature differences to be detected more easily.

On the first evaluation date (2 December 2016) (Figure 5(a)), plants under the DSV treatment displayed a mean canopy temperature of 31.9°C, while those submitted to NIRR and DSR treatments revealed mean canopy temperatures equal to 29.6 °C and 30.3°C, respectively. In turn, plants under the IRR treatment indicated the lowest mean canopy

temperature (25.5°C). The difference between the highest and lowest recorded canopy temperature (DSV and IRR, respectively) was 6.4°C, as evidenced by the thermal image obtained on such a date (Figure 6). In a previous study conducted in the same experimental area and involving the same treatments and plants at the same phenological stage (around 40 days after sowing – DAS), Crusiol et al. (2017) observed differences of 6°C among previously mentioned treatments, based on measurements attained via a handheld infrared thermometer. As per the canopy temperature, NRCT was higher in plants under the DSV treatment and lower under IRR and displayed intermediate values under DSR and NIRR (Figure 5(b)).

Differences between the temperature and NRCT values observed among the treatments are related to VPD during the evaluation period (1.01 kPa) and soil moisture content. Transpiration enables plants to maintain their temperature balance due to heat dissipation, thus preventing their intense heating. In soybean plants, transpiration is regulated by VPD (Seversike et al. 2013; Devi, Taliercio, and Sinclair 2015). Thus, an increase in VPD leads to a decrease in stomatal conductance (Wilson and Bunce 1997; Nakano et al. 2015) in order to prevent excessive transpiration. In this way, plants grown under appropriate water availability (e.g. the IRR treatment) present higher transpiration rates and hence leaf cooling, while plants under water withholding (e.g., the treatment DSV) display higher temperatures due to stomatal closure and lower transpiration rates.

These statements are corroborated by the soil moisture content obtained on 24 November 2016 (Figure 7) at 0 cm – 20 cm and 0–40 cm depths. On this date, plants submitted to the IRR treatment showed the highest soil moisture content, while those under NIRR and DSR presented intermediate values, and those under DSV the lowest values. Considering that between 24 November 2016 and 2 December 2016 the weather station recorded 46.1 mm rainfall and irrigation totalled 14.4 mm and taking into account that gravimetric analysis was performed prior to aerial thermal imaging, soil moisture content tended to decrease in DSV plots, but remained at higher levels in other treatments. This can be confirmed on the second date of soil moisture measurement (16 December 2016) (Figure 7).

The fact that leaf temperature was higher than air temperature indicates the occurrence of drought stress (Carvalho et al. 2015). Thus, in the present study, on the first evaluation date (2 December 2016) (Figure 5(a)), only plants submitted to the IRR treatment were not under drought stress. The occurrence of drought stress in the NIRR and DSR treatments, which only received water from rainfall, can be explained by the climatic

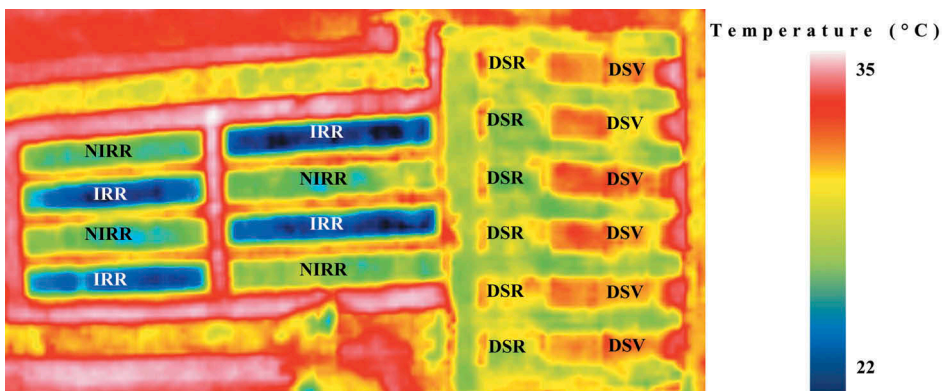


Figure 6. Thermal image obtained by an UAV thermal infrared camera on 2 December 2016.

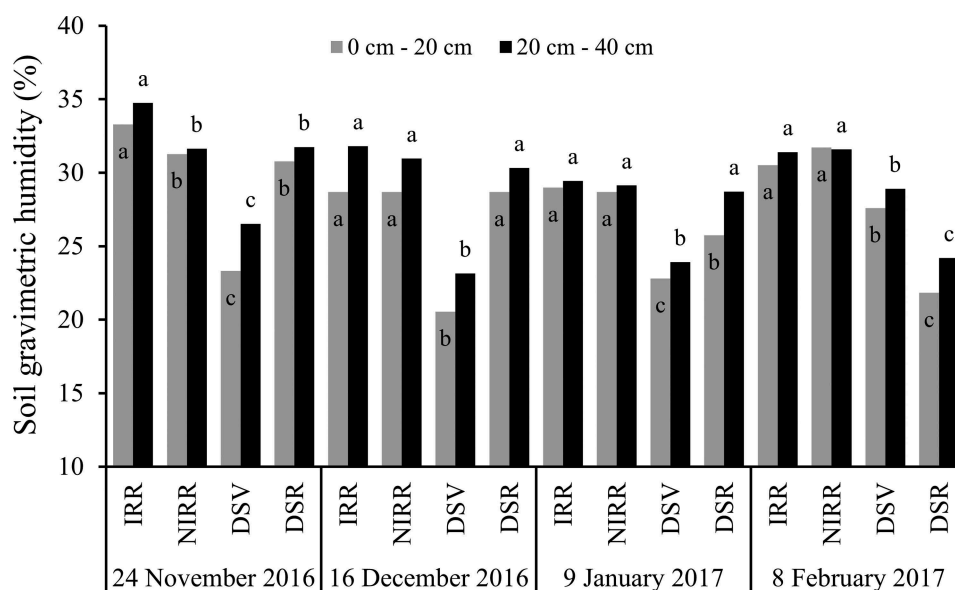


Figure 7. Soil moisture content (%) at 0 cm – 20 cm and 20 cm – 40 cm depths in the 2016–2017 crop season. Means followed by the same letter among treatments within each depth and on each date do not differ by Tukey test ($p \leq 0.05$).

water balance (Figure 8). Thus, a period of climatic water deficit was recorded on the three 10-day periods prior to evaluation (November), and so the available soil water did not meet the water requirements of the plants. A reduction in transpiration subsequently occurred, leading to an increase in leaf temperature.

On 12 December 2016, plants transferred from the vegetative to the reproductive stage. Thus, plants under DSV, which had previously been submitted to total water withholding, started to receive rainfall once again. In contrast, plants under DSR, which had previously received rainfall, were submitted to total water withholding (Figure 2(a)).

The second date of thermal image acquisition through UAV was 15 December 2016 (Figure 5), while soil moisture content was measured on 16 December 2016 (Figure 7), hence no rainfall was detected on these dates. Furthermore, from 12 to 15 December 2016, a period between the onset of drought stress at the reproductive stage and evaluation, only 3.9 mm rainfall was recorded. On 16 December 2016, the soil moisture content was similar at both evaluated depths, with the lowest values observed in the DSV treatment (Figure 7).

At this second thermal image acquisition, the difference between the highest and lowest canopy temperature was 5.2°C, with 0.82 kPa VPD. Plants under the DSV treatment, which had previously been submitted to water deficit, presented the highest canopy temperature and NRCT, i.e., 26.4°C and 0.9, respectively. Canopy temperatures under IRR, NIRR and DSR treatments were similar, which may be due to the rainfall volume (81.5 mm) recorded by the weather station between 2 and 15 December 2016 (Figure 8), hence no irrigation was performed in this period, resulting in a standardized soil moisture content in such treatments (Figure 7).

On the third evaluation date (27 December 2016) (Figure 5), the VPD was smaller (0.64 kPa) than on the previous assessment date. Plants under the DSV treatment showed the highest

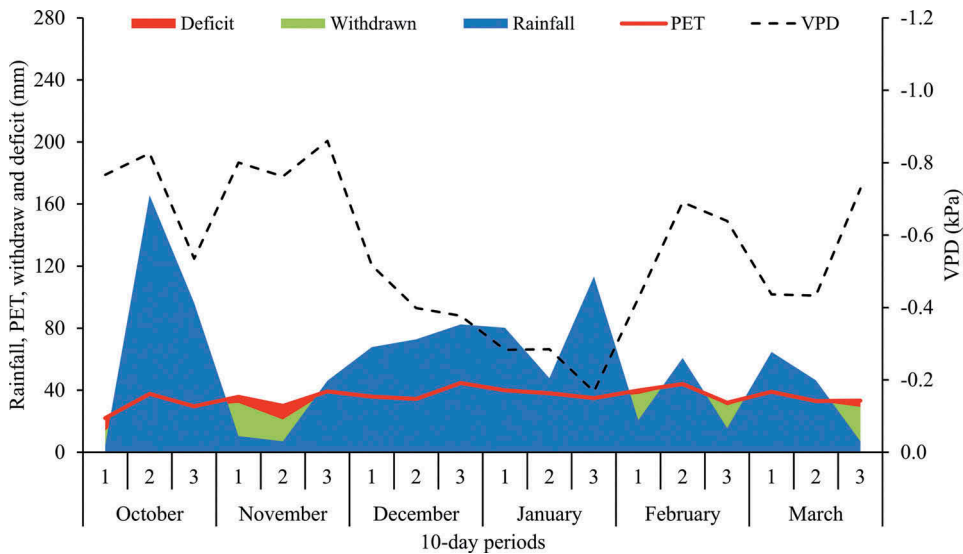


Figure 8. Climatic water balance at 10-day periods in the 2016–2017 crop season. Londrina-PR. PET: potential evapotranspiration; VPD: vapour pressure deficit.

canopy temperature and NRCT obtained through thermal images on 27 December 2016, and this was the only treatment that statistically differed. The greatest difference between the highest and lowest canopy temperature (7.2°C) was observed on this date between the IRR and DSV treatments. Rao (1985) obtained similar results regarding differences in temperature between soybean plants under drought stress and under continuous irrigation. He observed a difference of 8°C between such treatments.

Although soil moisture content was not measured on this date, the IRR and NIRR treatments showed the highest values at 0 cm – 20 cm and 20 cm – 40 cm depths based on measurements on 9 January 2017 (Figure 7). In turn, the DSR treatment revealed a decline in soil moisture content at 0 cm – 20 cm depth due to water withholding, but this did not differ from IRR and NIRR at 20 cm – 40 cm. The DSV treatment presented the lowest soil moisture content at the two evaluated depths.

Thus, according to the values of soil moisture content recorded on 16 December 2016 and 9 January 2017 (Figure 7), although DSV plots received 69.1 mm rainfall from 16 to 27 December 2016, their soil moisture content was nevertheless lower than that of the other treatments, and plants suffered drought stress because the canopy temperature was higher than the air temperature. In turn, although DSR plots did not receive 69.1 mm rainfall, they only presented changes in soil moisture content at 0 cm – 20 cm depth, while high values continue to be detected at 20 cm – 40 cm. Thus, soil moisture content corroborates the thermal behaviour of treatments.

Higher canopy than air temperatures were not observed in any of the three subsequent evaluations (Figure 5(a)), most likely due to the absence of climatic water deficit and small VPD values (Figure 8).

The fourth evaluation was performed on 11 January 2017 (Figure 5(a,b)). Although very close to 9 January 2017 (when soil moisture was measured), 35.8 mm rainfall was recorded between the two dates.

A small difference (2°C) between the highest and lowest canopy temperature was observed between the treatments on this date, most likely due to low VPD during the evaluation period (0.41 kPa). It must be emphasized that plants under the DSV treatment showed similar canopy temperature and NRCT than the treatments irrigated and non-irrigated, thus demonstrating that the plants were capable of recovering their previously impaired water status by a prolonged period of water withholding to which they had been submitted.

In a previous study conducted at the same experimental site but using a handheld infrared thermometer, Crusiol et al. (2017) observed a slightly lower canopy temperature in plants submitted to the DSV treatment than of plants under IRR at the reproductive stage.

On this evaluation date (11 January 2017) the thermal behaviour of plants might be related to soil water availability and LAI, measured on 16 January 2017 (Figure 9(a)).

Such a reduction in leaf area leads to a reduction in the total area for transpiration. Thus, soil water availability in DSV plots (Figure 7), whilst still lower than in the case of IRR and NIRR, was sufficient to maintain stomatal opening, leading to a higher transpiration rate and greater plant cooling. Thereupon, a higher transpiration rate in relation to leaf area probably occurred in DSV plots relative to other treatments on this date, resulting in a lower canopy temperature. Furthermore, a lower LAI observed in DSV plots may have contributed to facilitate canopy cooling, thus enabling plants to show greater thermal energy dissipation due to higher air circulation within the canopy. Another possible explanation is that plants under the DSV treatment developed a wider and deeper root system (data not shown) since they were submitted to water deficit at the vegetative stage. Thus, these plants would be capable of counterbalancing low water availability in the upper and intermediate soil layers by presenting superior water uptake in deeper soil, thus maintaining transpiration and lower leaf temperatures on the final three evaluation dates.

This same thermal behaviour – a lower canopy temperature in DSV plots – was observed on the following two evaluation dates, i.e., 16 January 2017 and 8 February 2017.

On 16 January 2017, the date when the fifth evaluation was performed (Figure 5), significant differences in canopy temperature and NRCT could not be detected between treatments. The lowest mean canopy temperature and NRCT were observed under DSV (16.55°C and 0.31, respectively), while the highest were detected in plants under the DSR treatment (16.75°C and 0.81, respectively). On this date, the lowest difference in temperature (0.2°C) was observed among treatments, most likely due to VPD (0.30 kPa), which was the

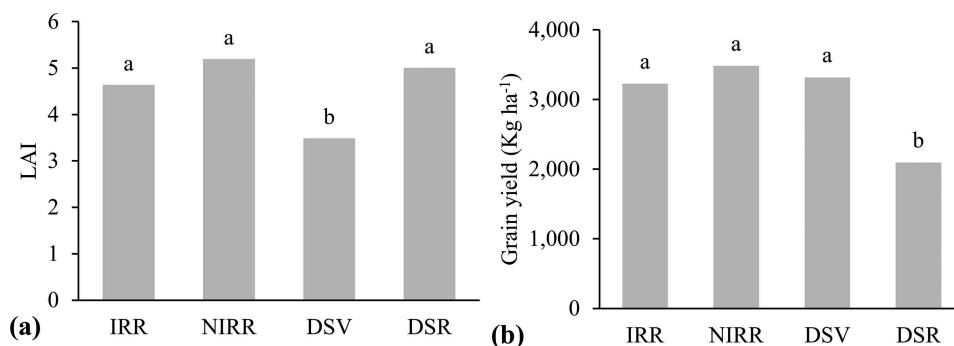


Figure 9. Leaf area index (a) measured on 16 January 2017 and grain yield in the 2016–2017 crop season (b, Kg ha⁻¹). Means followed by the same letter do not differ by Tukey test ($p \leq 0.05$).

lowest among all evaluations (Figure 8). Once again, our data confirm the relationship between the transpiration of soybean plants and VPD (Seversike et al. 2013; Devi, Taliercio, and Sinclair 2015) and between the transpiration of soybean plants and stomatal conductance (Wilson and Bunce 1997; Nakano et al. 2015). Thus, it must be emphasized that small VPD (0.30 kPa) may have resulted in a wide stomatal opening and consequently leaf cooling in all treatments.

On the final evaluation date (8 February 2017), significant differences in canopy temperature and NRCT were detected among the treatments (Figure 5). As expected, plants under the DSR treatment, which were submitted to drought stress over a period of 59 days and were thus deprived of 407.5 mm rainfall, showed the highest canopy temperature (26°C) and NRCT (0.94). On this date, a difference of 3°C was observed between treatments due to higher VPD (1.02 kPa) than in the previous evaluation. Again, plants under the DSV demonstrated the lowest canopy temperature (23.02°C) and the smallest NRCT (0.09) of all treatments (Figure 5).

On this evaluation date, soil moisture content was similar at 0 cm – 20 cm and 20 cm – 40 cm depths (Figure 7). DSR plots showed a higher canopy temperature because they had a lower soil moisture content. However, even DSV plots presented lower soil moisture content than that of IRR and NIRR treatments. The former showed a lower canopy temperature, strengthening the hypothesis of a relationship between lower LAI and higher transpiration.

These results suggest that the transpiration rates presented by plants under DSV were higher than those of the other treatments due to lower LAI, as the water stored in the soil fully meets the water requirements of such plants even under lower soil moisture content.

Figure 9(b) displays the grain yield of the 2016–2017 crop season. Although plants under the DSV treatment had been submitted to water deficit, they revealed a similar grain yield to that of IRR and NIRR. In turn, in plants under DSR, whilst they did not present a higher canopy than air temperature, water withholding at the crop development stage was most sensitive to water scarcity and resulted in a lower grain yield than in the other treatments.

Soybean plants under drought stress at the vegetative stage tended to present a high grain yield, similar to that obtained in plants under natural conditions or irrigation. However, among plants submitted to drought stress at the reproductive stage, grain yield was significantly lower than was the case of plants under water deficit induced at the vegetative stage under either natural conditions or irrigation. Thus, water withholding at the reproductive stage was more harmful to soybean production, as has also been reported by several authors in studies evaluating soybean plants submitted to different water availability levels (Nogueira and Nagai 1988; de Paiva Rolla et al. 2014; Carvalho et al. 2015; Crusiol et al. 2017).

In the 2017–2018 crop season, the relationship between canopy temperature and soil water availability was similar to that observed in the previous crop season. Figure 10 presents the values of canopy temperature (a) and NRCT (b) for the 2017–2018 crop season.

At the first evaluation date, 29 November 2017, no statistical difference was detected between treatments in canopy temperature or NRCT. The absence of differences is related to: the short period (9 days) to which DSV was submitted to water deficit, even though this treatment had been deprived of 48.1 mm of rainfall; the non-necessity of irrigation (Figure 2(b)); and the VPD at the moment of thermal image acquisition (0.44 kPa, the smallest among evaluation dates), a trend previously observed on 16 January 2017 (Figure 5(a)), when VPD may have led to a wide stomatal opening, resulting in leaf cooling in all treatments.

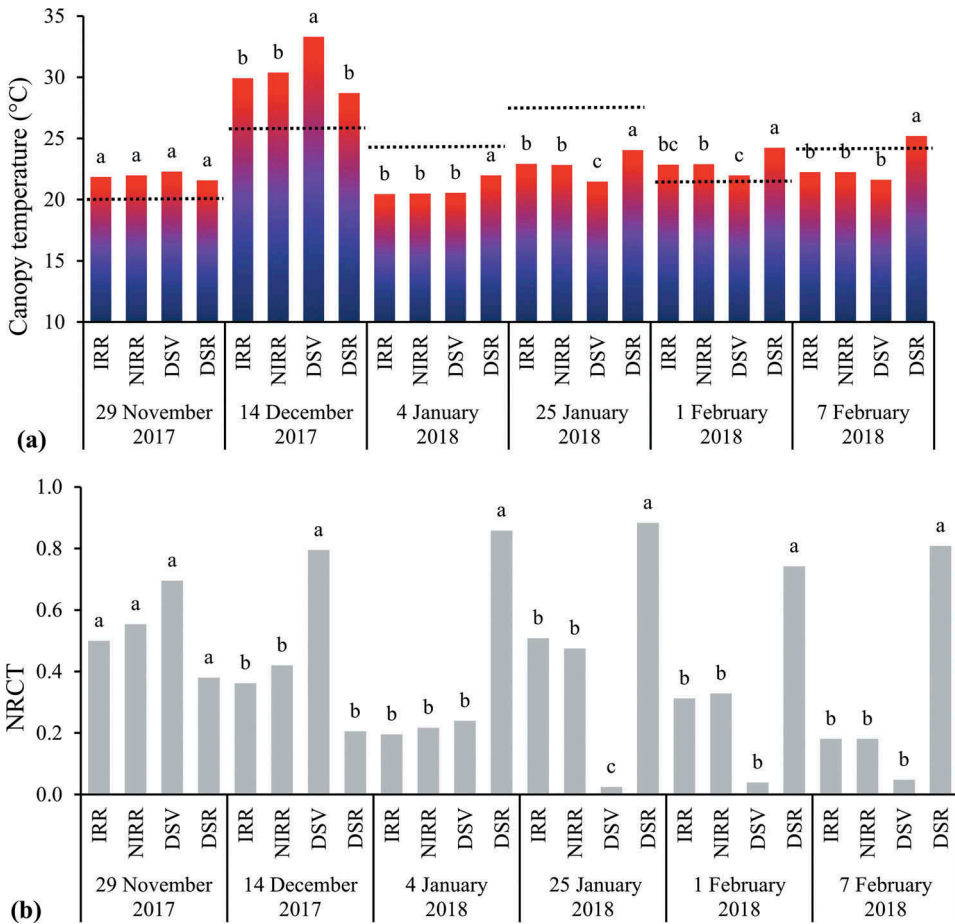


Figure 10. Canopy temperature (a) and NRCT (b) in the 2017–2018 crop season. Dashed lines represent air temperature (°C) on each date. Means followed by the same letter among treatments within each date do not differ by Tukey test ($p \leq 0.05$).

Although soil moisture content was measured five days later, between this date and 4 December 2017, rainfall was not reported, and the soil moisture content (Figure 11) tended to decline on DSV plots at both depths.

During the period from the onset of the drought stress in the DSV treatment (20 November 2017) to the second evaluation date (14 December 2017), the rainfall recorded within the experimental area was 71.4 mm. At the second evaluation date, the DSV treatment showed the lowest soil moisture content (Figure 11) and consequently the highest canopy temperature (33.3°C) and NRCT (0.79) (Figure 10). Differences in canopy temperature and NRCT among the other three treatments were not detected due to the similarity of conditions to which they were submitted, receiving only rainfall (Figure 2(b)).

Regarding canopy temperature, three interesting phenomena were observed on this evaluation date. First, canopy temperatures were far higher than on the other evaluation dates; second, canopy temperatures within the evaluation date were higher than air temperatures; third, the largest temperature difference (4.6°C) was detected between the

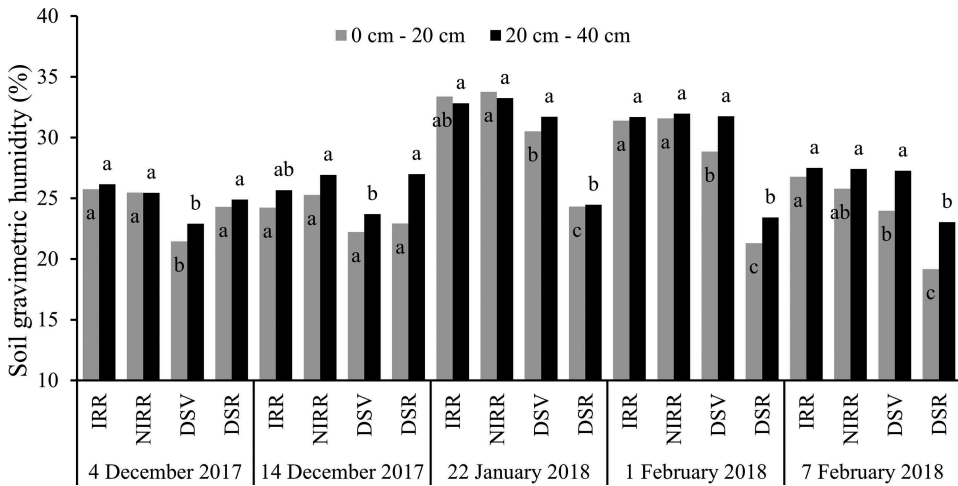


Figure 11. Soil moisture content (%) at 0 cm – 20 cm and 20 cm – 40 cm depths in the 2017–2018 crop season. Means followed by the same letter among treatments within each depth on each date do not differ by Tukey test ($p \leq 0.05$).

treatments (DSV vs DSR). This thermal behaviour is probably related to the low accumulated rainfall during the previous 10-day period (Figure 12) as well as to the VPD (0.93 kPa, the largest among evaluation dates). Moreover, as was also observed in the 2016–2017 crop season (2 December 2016 – Figure 5(a)), such conditions resulted in stomatal closure even under good conditions of water availability in order to avoid excessive transpiration, resulting in lower heat dissipation and a high canopy temperature.

On 19 December 2017, plants transferred from the vegetative to the reproductive stage. Thus, the DSV treatment, which had previously been subjected to total water withholding,

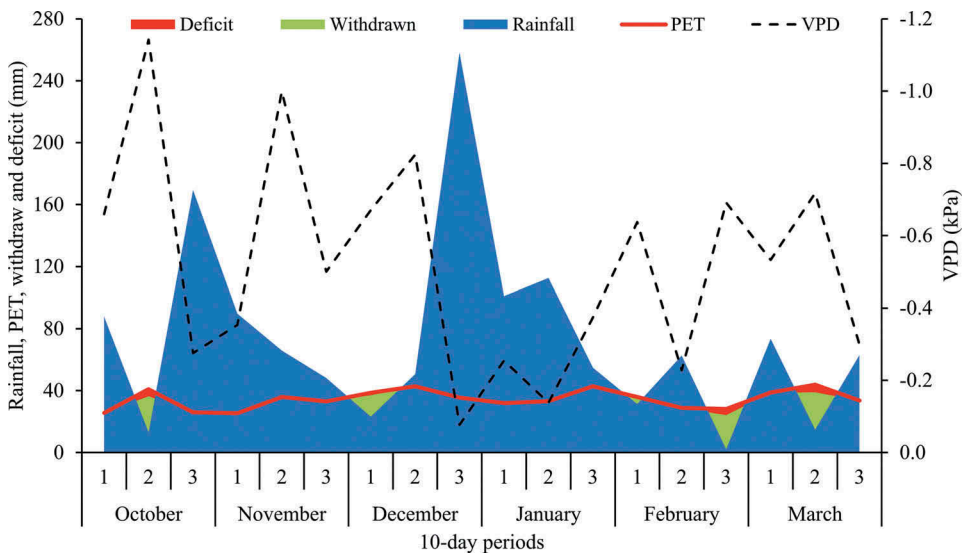


Figure 12. Climatic water balance at 10-day periods in the 2017–2018 crop season. Londrina-PR. PET: potential evapotranspiration; VPD: vapour pressure deficit.

again received rainfall, while the DSR treatment, which had previously received rainfall, altered to a total water withholding condition (Figure 2(b)). In this way, on 4 January 2018 the canopy temperature and NRCT of DSV did not differ between IRR and NIRR treatments, and the highest canopy temperature was detected on DSR (Figure 10).

The decrease and increase in the canopy temperature of DSV and DSR respectively is due to the large volume of rainfall accumulated since the rainout shelter inversion (19 December 2017): 340.8 mm. Thus, although soil moisture content was not measured on this date, it is feasible that owing to the large amount of rainfall, the soil moisture content increased on DSV and decreased on DSR. This is corroborated by the soil moisture content accessed on 22 January 2018 (Figure 11).

On the final three evaluation dates (25 January and 1 and 7 February 2018), DSR, which presented a lower soil moisture content (Figure 11), displayed the highest canopy temperature and NRCT. This indicates that on 1 February 2018 the canopy temperature was higher than the air temperature, suggesting the occurrence of drought stress.

On both 22 January and 1 February 2018, the DSV treatment showed a lower soil humidity content than IRR and NIRR at a depth of 0 cm – 20 cm (Figure 11), but lower canopy temperatures and NRCT than the other treatments (Figure 10), following the same trend discussed in the 2016–2017 crop season (11 January – Figure 5).

This trend was also observed on the final evaluation date (7 February 2018), when DSV presented a lower soil moisture content than IRR and NIRR (Figure 11) at both depths, but a similar canopy temperature and NRCT (Figure 10). This supports the hypothesis that even though plants in DSV reduced their leaf area under lower soil humidity content than IRR and NIRR, they were able to maintain stomatal opening, resulting in higher transpiration rates by total leaf area and superior heat dissipation via increased air circulation within the canopy. In addition, the stress in the early stages may have promoted a broader and deeper root system, which was able to supply enough water to keep the canopy temperature low.

Observations performed from the end of water withholding in DSV in both the 2016–2017 and 2017–2018 crop seasons reveal that plants submitted to water deficit in the vegetative stages and subsequently rehydrated from the onset of the reproductive stages displayed a lower canopy temperature and NRCT than treatments under appropriate water availability (IRR and NIRR).

In 2017–2018, soybean plants under the DSR treatment were submitted to 51 days of water withholding and were deprived of 562.7 mm of rainfall. Consequently, yields were reduced to less than half of the other treatments (Figure 13). Once again, the DSV, previously subjected to complete water withholding in the vegetative stages, showed a similar grain yield as treatments under normal field conditions, receiving only rainfall (e.g. irrigated and non-irrigated).

These results reaffirm that when water deficit occurs in the reproductive stages of soybean development, it is more harmful to grain yield than its occurrence in the vegetative stages.

The grain yield of the evaluated treatments presented significant differences between the 2016–2017 and 2017–2018 crop seasons, with significant interaction between 'treatment' and 'crop season' factors. These values may have been influenced by climatological elements, with different amounts and distributions of rainfall (Figures 8 and 12), as well as other elements, such as global solar radiation. Consequently, the applicability of the methodology used in this study is strengthened because it can be applied to crop seasons with different climatological conditions.

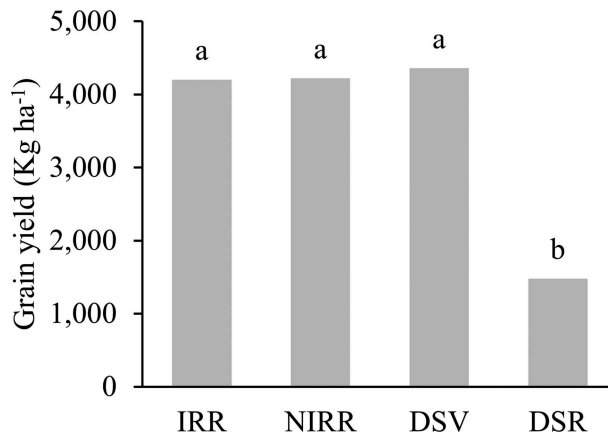


Figure 13. Grain yield in the 2017–2018 crop season (Kg ha⁻¹). Means followed by the same letter do not differ by Tukey test ($p \leq 0.05$).

4. Conclusions

The use of thermal images obtained through an UAV thermal infrared camera is subject to the interference of several methodological factors. In the present study, thermal infrared radiation attenuation by the atmosphere reduced the temperature recorded by the sensor at 100 m AGL by up to 16°C. Furthermore, such attenuation showed a positive linear correlation with flight altitude. Thus, images of the same target acquired at ground and above ground level and the consequently acquisition of a correction factor enable the elimination of atmospheric attenuation.

Thermal imaging and NRCT were efficient in distinguishing the water status of soybean plants in both crop seasons evaluated, marked by different climatological conditions. The results indicate that the thermal behaviour of soybean plants is directly related to soil moisture and VPD. Under low VPD, the thermal capacity for discriminating plant canopies was less evident or could not be performed, only displaying 0.2°C amplitude. In turn, at higher VPD values, differences of up to 7.2°C were observed. Regarding soil water availability (represented by soil moisture content), higher values corresponded to lower canopy temperatures, while lower soil moisture content corresponded to higher canopy temperatures. However, it must be emphasized that VPD was a determining factor for the detection of thermal differences among treatments.

Soybean plants submitted to water deficit at the vegetative stages and subsequently rehydrated saw their water requirements fully met, even with lower soil water supply. The reasons might include a reduction in leaf area, greater thermal energy dissipation due to higher air circulation within the canopy, and the potential development of a wider and deeper root system that provides superior soil water uptake, resulting in lower temperatures than in plants without water restrictions during the entire crop cycle.

Thus, the treatments evaluated in the present study indicated that water deficit was most severe at the reproductive stage, leading to a lower grain yield. However, at the vegetative stage, grain yield was similar to that of treatments under continuous irrigation or exposed to rainfall.

The procedure adopted to calculate NRCT was satisfactory because it described plant water status as identified in the field. Instead of adopting theoretical limits to its calculation, the treatments provided real values for such an index, enabling NRCT to apply a contrast on canopy temperature values, contributing to a greater understanding of the results.

Finally, we emphasize the lack of studies regarding the water status of soybean plants through UAV-based aerial thermal imaging. This paper demonstrates the significant potential of using UAV thermal infrared cameras to monitor the water status of soybean plants, providing non-destructive and quick measurements and allowing the extrapolation of obtained information to new study areas.

Acknowledgements

This work was supported by the [National Council for Scientific and Technological Development – CNPq] and [Coordination for the Improvement of Higher Education Personnel – CAPES].

Disclosure statement

No potential conflict of interest was reported by the authors.

Funding

This work was supported by the Conselho Nacional de Desenvolvimento Científico e Tecnológico (CNPq); Coordenação de Aperfeiçoamento de Pessoal de Nível Superior (CAPES).

ORCID

Luís Guilherme Teixeira Crusiol  <http://orcid.org/0000-0002-2387-964X>

Marcos Rafael Nanni  <http://orcid.org/0000-0003-4854-2661>

References

- Alchanatis, V., Y. Cohen, S. Cohen, M. Moller, M. Sprinstin, M. Meron, J. Tsipris, Y. Saranga, and E. Sela. 2010. "Evaluation of Different Approaches for Estimating and Mapping Crop Water Status in Cotton with Thermal Imaging." *Precision Agriculture* 11: 27–41. doi:10.1007/s11119-009-9111-7.
- Alvares, C. A., J. L. Stape, P. C. Sentelhas, J. L. Gonçalves, and S. G. de Moraes. 2013. "Köppen's Climate Classification Map for Brazil." *Meteorologische Zeitschrift* 22: 711–728. doi:10.1127/0941-2948/2013/0507.
- Baluja, J., M. P. Diago, P. Balda, R. Zorer, F. Meggio, F. Morales, and J. Tardaguila. 2012. "Assessment of Vineyard Water Status Variability by Thermal and Multispectral Imagery Using an Unmanned Aerial Vehicle (UAV)." *Irrigation Science* 30: 511–522. doi:10.1007/s00271-012-0382-9.
- Bellvert, J., P. J. Zarco-Tejada, J. Girona, and E. Fereres. 2014. "Mapping Crop Water Stress Index in a 'pinot-noir' Vineyard: Comparing Ground Measurements with Thermal Remote Sensing Imagery from an Unmanned Aerial Vehicle." *Precision Agriculture* 15: 361–376. doi:10.1007/s11119-013-9334-5.
- Bellvert, J., P. J. Zarco-Tejada, J. Marsal, J. Girona, V. González-Dugo, and E. Fereres. 2015. "Vineyard Irrigation Scheduling Based on Airborne Thermal Imagery and Water Potential Thresholds." *Australian Journal of Grape and Wine Research* 22: 307–315. doi:10.1111/ajgw.12173.

- Berni, J. A., P. J. Zarco-Tejada, L. Suárez, and E. Fereres. 2009a. "Thermal and Narrowband Multispectral Remote Sensing for Vegetation Monitoring from an Unmanned Aerial Vehicle." *IEEE Transactions on Geoscience and Remote Sensing* 47: 722–738. doi:10.1109/TGRS.2008.2010457.
- Berni, J. A. J., P. J. Zarco-Tejada, G. Sepulcre-Cantó, E. Fereres, and F. Villalobos. 2009b. "Mapping Canopy Conductance and CWSI in Olive Orchards Using High Resolution Thermal Remote Sensing Imagery." *Remote Sensing of Environment* 113: 2380–2388. doi:10.1016/j.rse.2009.06.018.
- Carvalho, J. D. F. C., L. G. T. Crusiol, L. J. Perini, R. N. R. Sibalidelli, L. C. Ferreira, F. C. Marcelino-Guimarães, A. L. Nepomuceno, N. Neumaier, and J. R. B. Farias. 2015. "Phenotyping Soybeans for Drought Responses Using Remote Sensing Techniques and Non-destructive Physiological Analysis." *Global Science and Technology* 8: 1–16. doi:10.14688/1984-3801/gst.v8n2p1-16.
- CONAB (National Company of Food Supply). 2018. "Brazilian Crop Assessment – Grain, 2017/2018 Crops, Seventh Inventory Survey, April/2018." <https://www.conab.gov.br/index.php/info-agro/safras>
- Crusiol, L. G. T., J. D. F. C. Carvalho, R. N. R. Sibalidelli, W. Neiverth, A. Do Rio, L. C. Ferreira, S. O. de Procópio, et al. 2017. "NDVI Variation according to the Time of Measurement, Sampling Size, Positioning of Sensor and Water Regime in Different Soybean Cultivars." *Precision Agriculture* 18: 470–490. doi:10.1007/s11119-016-9465-6.
- de Paiva Rolla, A. A., J. D. F. C. Carvalho, R. Fuganti-Pagliarini, C. Engels, A. Do Rio, S. R. R. Marin, M. C. N. de Oliveira, et al. 2014. "Phenotyping Soybean Plants Transformed with rd29A: AtDREB1A for Drought Tolerance in the Greenhouse and Field." *Transgenic Research* 23: 75–87. doi:10.1007/s11248-013-9723-6.
- Devi, M. J., E. W. Taliércio, and T. R. Sinclair. 2015. "Leaf Expansion of Soybean Subjected to High and Low Atmospheric Vapour Pressure Deficits." *Journal of Experimental Botany* 66: 1845–1850. doi:10.1093/jxb/eru520.
- Elsayed, S., M. Elhoweity, H. H. Ibrahim, Y. H. Dewir, H. M. Migdadi, and U. Schmidhalter. 2017. "Thermal Imaging and Passive Reflectance Sensing to Estimate the Water Status and Grain Yield of Wheat under Different Irrigation Regimes." *Agricultural Water Management* 189: 98–110. doi:10.1016/j.agwat.2017.05.001.
- Elsayed, S., P. Rischbeck, and U. Schmidhalter. 2015. "Comparing the Performance of Active and Passive Reflectance Sensors to Assess the Normalized Relative Canopy Temperature and Grain Yield of Drought-stressed Barley Cultivars." *Field Crops Research* 177: 148–160. doi:10.1016/j.fcr.2015.03.010.
- Elvanidi, A., N. Katsoulas, T. Bartzanas, K. P. Ferentinos, and C. Kittas. 2017. "Crop Water Status Assessment in Controlled Environment Using Crop Reflectance and Temperature Measurements." *Precision Agriculture* 18: 332–349. doi:10.1007/s11119-016-9492-3.
- Embrapa Soja. 2013. *Tecnologias De Produção De Soja – Região Central Do Brasil 2014*. Londrina: Embrapa Soja.
- Faye, E., F. Rebaudo, D. Yáñez-Cajo, S. Cauvy-Fraunié, and O. Dangles. 2016. "A Toolbox for Studying Thermal Heterogeneity across Spatial Scales: From Unmanned Aerial Vehicle Imagery to Landscape Metrics." *Methods in Ecology and Evolution* 7: 437–446. doi:10.1111/2041-210X.12488.
- Fehr, W. R., and C. E. Caviness. 1977. "Stages of Soybean Development". *Special Report* 80. Iowa: Iowa State University of Science and Technology.
- Ferreira, D. F. 2011. "Sisvar: A Computer Statistical Analysis System." *Ciência E Agrotecnologia (UFPA)* 35: 1039–1042. doi:10.1590/S1413-70542011000600001.
- Ferreira, R. C. 2016. "Quantificação Das Perdas Por Seca Na Cultura Da Soja O Brasil." PhD Thesis, Universidade Estadual de Londrina.
- Gates, D. M. 1964. "Leaf Temperature and Transpiration." *Agronomy Journal* 56: 273–277. doi:10.2134/agronj1964.00021962005600030007x.
- Gómez-Candón, D., N. Virlet, S. Labbé, A. Jolivot, and J. L. Regnard. 2016. "Field Phenotyping of Water Stress at Tree Scale by UAV-sensed Imagery: New Insights for Thermal Acquisition and Calibration." *Precision Agriculture* 17: 786–800. doi:10.1007/s11119-016-9449-6.
- Gonzalez-Dugo, V., P. Zarco-Tejada, E. Nicolás, P. A. Nortes, J. J. Alarcón, D. S. Intrigliolo, and E. Fereres. 2013. "Using High Resolution UAV Thermal Imagery to Assess the Variability in the

- Water Status of Five Fruit Tree Species within a Commercial Orchard." *Precision Agriculture* 14: 660–678. doi:10.1007/s11119-013-9322-9.
- Idso, S. B., R. D. Jackson, P. J. Pinter, R. J. Reginato, and J. L. Hatfield. 1981. "Normalizing the Stress-degree-day Parameter for Environmental Variability." *Agricultural Meteorology* 24: 45–55. doi:10.1016/0002-1571(81)90032-7.
- Jackson, R. D., S. B. Idso, R. J. Reginato, and P. J. Pinter. 1981. "Canopy Temperature as a Crop Water Stress Indicator." *Water Resources Research* 17: 1133–1138. doi:10.1029/WR017i004p01133.
- Jackson, R. D., W. P. Kustas, and B. J. Choudhury. 1988. "A Reexamination of the Crop Water Stress Index." *Irrigation Science* 9: 309–317. doi:10.1007/BF00296705.
- Jones, H. G. 1999. "Use of Thermography for Quantitative Studies of Spatial and Temporal Variation of Stomatal Conductance over Leaf Surfaces." *Plant, Cell and Environment* 22: 1043–1055. doi:10.1046/j.1365-3040.1999.00468.x.
- Jones, H. G., M. Stoll, T. Santos, C. D. Sousa, M. M. Chaves, and O. M. Grant. 2002. "Use of Infrared Thermography for Monitoring Stomatal Closure in the Field: Application to Grapevine." *Journal of Experimental Botany* 53: 2249–2260. doi:10.1093/jxb/erf083.
- Lillesand, T. M., R. W. Kiefer, and J. W. Chipman. 2004. *Remote Sensing and Image Interpretation*. New York: John Wiley & Sons, Inc.
- Maes, W. H., A. R. Huete, and K. Steppe. 2017. "Optimizing the Processing of UAV-Based Thermal Imagery." *Remote Sensing* 9: 476. doi:10.3390/rs9050476.
- Mengistu, A., H. Tachibana, A. H. Epstein, K. G. Bidne, and J. D. Hatfield. 1987. "Use of Leaf Temperature to Measure the Effect of Brown Stem Rot and Soil Moisture Stress and Its Relation to Yields of Soybeans." *Plant Disease* 71: 632–634. doi:10.1094/PD-71-0632.
- Nakano, S., C. R. Tacarindua, K. Nakashima, K. Homma, and T. Shiraiwa. 2015. "Evaluation of the Effects of Increasing Temperature on the Transpiration Rate and Canopy Conductance of Soybean by Using the Sap Flow Method." *Journal of Agricultural Meteorology* 71: 98–105. doi:10.2480/agrmet.D-14-00046.
- Nogueira, S. S., and V. Nagai. 1988. "Deficiência Hídrica Simulada Nos Diferentes Estádios De Desenvolvimento De Um Cultivar Precoce De Soja." *Bragantia* 47: 9–14. doi:10.1590/S0006-87051988000100002.
- Rao, T. V. R. 1985. "Monitoring Water Stress in Soybean Plants with Remote Sensing Techniques." PhD Thesis, University of Nebraska.
- Ritter, M. 2017. "Further Development of an Open-source Thermal Imaging System in Terms of Hardware, Software and Performance Optimizations." PhD Thesis, University of Applied Sciences Pforzheim.
- Sentelhas, P. C., R. Battisti, G. M. S. Câmara, J. R. B. Farias, A. C. Hampf, and C. Nendel. 2015. "The Soybean Yield Gap in Brazil—Magnitude, Causes and Possible Solutions for Sustainable Production." *The Journal of Agricultural Science* 153: 1394–1411. doi:10.1017/S0021859615000313.
- Sepulcre-Cantó, G., P. J. Zarco-Tejada, J. C. Jiménez-Muñoz, J. A. Sobrino, E. de Miguel, and F. J. Villalobos. 2006. "Detection of Water Stress in an Olive Orchard with Thermal Remote Sensing Imagery." *Agricultural and Forest Meteorology* 136: 31–44. doi:10.1016/j.agrformet.2006.01.008.
- Seversike, T. M., S. M. Sermons, T. R. Sinclair, T. E. Carter, and T. W. Ruffy. 2013. "Temperature Interactions with Transpiration Response to Vapor Pressure Deficit among Cultivated and Wild Soybean Genotypes." *Physiologia Plantarum* 148: 62–73. doi:10.1111/j.1399-3054.2012.01693.x.
- Sibaldelli, R. N. R., and J. R. B. Farias. 2017. *Boletim Agrometeorológico Da Embrapa Soja, Londrina, PR – 2016*. Londrina: Embrapa Soja. <http://www.infoteca.cnptia.embrapa.br/infoteca/handle/doc/1067152>
- Sibaldelli, R. N. R., and J. R. B. Farias. 2018. *Boletim Agrometeorológico Da Embrapa Soja, Londrina, PR – 2017*. Londrina: Embrapa Soja. <https://www.infoteca.cnptia.embrapa.br/infoteca/handle/doc/1087963>
- Stolf-Moreira, R., E. G. M. Lemos, L. Carareto-Alves, J. Marcondes, S. S. Pereira, A. A. P. Rolla, R. M. Pereira, et al. 2011. "Transcriptional Profiles of Roots of Different Soybean Genotypes Subjected to Drought Stress." *Plant Molecular Biology Reporter* 29: 19–34. doi:10.1007/s11105-010-0203-3.

- Sullivan, D. G., J. P. Fulton, J. N. Shaw, and G. Bland. 2007. "Evaluating the Sensitivity of an Unmanned Thermal Infrared Aerial System to Detect Water Stress in a Cotton Canopy." *Transactions of the ASABE* 50: 1955–1962. doi:10.13031/2013.24091.
- Tetens, O. 1930. "Über Einige Meteorologische Begriffe. Z." *Geophys* 6: 297–309.
- Thorntwaite, C. W., and J. R. Mather. 1955. *The Water Balance*. Centerton: Laboratory of Climatology.
- United States Department of Agriculture (USDA). 2018. "World Agricultural Production. Circular Series WAP 4-18, April, 2018." <https://apps.fas.usda.gov/psdonline/circulars/production.pdf>
- Watson, D. J. 1947. "Comparative Physiological Studies in the Growth of Field Crops. I. Variation in Net Assimilation Rate and Leaf Area between Species and Varieties, and within and between Years." *Annals of Botany* 11: 41–76. doi:10.1093/oxfordjournals.aob.a083148.
- Wilson, K. B., and J. A. Bunce. 1997. "Effects of Carbon Dioxide Concentration on the Interactive Effects of Temperature and Water Vapour on Stomatal Conductance in Soybean." *Plant, Cell and Environment* 20: 230–238. doi:10.1046/j.1365-3040.1997.d01-58.x.
- Wrege, M. S., S. Steinmetz, C. Reiser Júnior, and I. R. de Almeida. 2011. *Atlas Climático Da Região Sul Do Brasil: Estados Do Paraná, Santa Catarina E Rio Grande Do Sul*. Pelotas: Embrapa Clima Temperado.
- Zarco-Tejada, P. J., V. González-Dugo, and J. A. Berni. 2012. "Fluorescence, Temperature and Narrow-band Indices Acquired from a UAV Platform for Water Stress Detection Using a Micro-hyperspectral Imager and a Thermal Camera." *Remote Sensing of Environment* 117: 322–337. doi:10.1016/j.rse.2011.10.007.
- Zarco-Tejada, P. J., V. González-Dugo, L. E. Williams, L. Suárez, J. A. Berni, D. Goldhamer, and E. Fereres. 2013. "A PRI-based Water Stress Index Combining Structural and Chlorophyll Effects: Assessment Using Diurnal Narrow-band Airborne Imagery and the CWSI Thermal Index." *Remote Sensing of Environment* 138: 38–50. doi:10.1016/j.rse.2013.07.024.